The realization of sub-nanosecond pump and probe experiments at the ESRF

Michael Wulff,[a] Anton Plech,[a] Laurent Eybert,[a] Rudolf Randler,[a] Friedrich Schotte[b] and Philip Anfinrud[b]

[a] *European Synchrotron Radiation Facility, 6 rue Jules Horowitz, BP 220, Grenoble Cedex, 38043, France*

[b] *Laboratory of Chemical Physics, NIDDK, National Institutes of Health, Building 5, Bethesda, MD, 20892-0520, USA*

Received 18th March 2002, Accepted 29th April 2002

We present beamline ID09B that is designed for pump and probe experiments to 50 ps time-resolution. The beamline has been refurbished with a narrow-bandwidth undulator for Laue diffraction and diffraction from liquids. The new undulator has 235 poles, a 17 mm magnetic period and is operated at 6.5 mm gap. It produces a spectral flux of 2.0×10^8 photon/0.1% bw/pulse (10 mA) at the fundamental at 15.5 keV and an integral flux of 1.1×10^{10} photon pulse^{-1} in a 2.5% bandwidth. The optics has been renewed with a high-precision toroidal mirror and a cryogenic monochromator. The X-ray chopper used for single pulse selection is also described together with the femtosecond laser. Finally the diffraction from excited iodine molecules in CCl_4 is investigated on the nanosecond time-scale. It turns out that the high-angle scattering is insensitive to the thermal chock from the laser; these oscillations are therefore readily used for structure determination. Conversely, the low-angle scattering probes the hydrodynamics of the liquid over longer length scales and the oscillations are believed to originate from thermal stress and expansion of the solvent.

1. Introduction

The intensity of the pulsed radiation from undulators from the European Synchrotron Radiation Facility (ESRF, 6 GeV), the Advanced Photon Source (APS, 7 GeV) and Spring8 (8 GeV), has made it possible to conduct pump and probe experiments on chemical and biochemical systems down to a time-resolution of 50–200 ps. In these machines, the undulators produce polychromatic beams with a spectrum of harmonics caused by the interference of single electrons.[1] The spectrum of the new U17 undulator from beamline ID09 at the ESRF is shown in Fig. 1. The figure shows the spectral flux, *i.e.* the photon count in a 0.1% bandwidth, as produced by one bunch of electrons traversing the insertion device (10 mA single-bunch mode). The bunch contains 1.8×10^{11} electrons and produces 1.1×10^{10} photons in 145 ps (fwhm)! Although the pulse length is a thousand times longer than the time it takes to form and break chemical bonds, the intensity is orders of magnitude greater than from second generation synchrotrons and rotating anodes. Plasma sources can provide sub-picosecond pulses and deliver up to 5×10^4 photon pulse^{-1} on the sample[2] and that is sufficient for surface studies but insufficient for biological molecules. So until the arrival of the

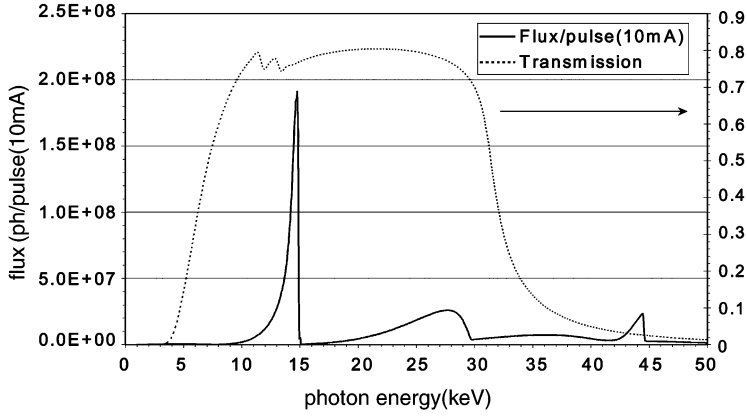

Fig. 1 Spectral intensity of the in-vacuum undulator U17 from a single bunch (10 mA, 28.2 nC/bunch). The apertures in the calculation have been set to accept 99% of the central cone. The transmission of the front-end, the beamline beryllium window and the toroidal mirror at 2.68 mrad are shown to the right.

X-ray free electron laser towards 2010, third generation synchrotrons are the only source for time-resolved experiments in chemical and biochemical systems.

We have used the short X-ray pulses to probe the moving structure of molecules that have been initiated by a short laser pulse. The experiments use pump and probe: a short optical pulse initiates the molecules and a delayed X-ray pulse takes a snapshot of the moving structure at a given delay. The scattering pattern is normally recorded on a CCD detector and the experiment repeated for improved statistics. The experimental methods that have been developed include Laue diffraction from macromolecules,[3–5] diffraction from smaller molecules[6] and diffraction from liquids.[7,8] The Laue program has benefited enormously from having abandoned the wiggler approach with a narrow-bandwidth undulator, the latter of which gives much superior data quality.[9] In addition it is also very fortuitous that many reactions are active in the crystal. That makes it possible to construct the three-dimensional electron density in sharp contrast to the one-dimensional information from a liquid.

A high integral-flux per pulse is of crucial importance for these studies since it reduces the exposure time and makes the data less sensitive to drifts and radiation damage. For these reasons we have upgraded the ID09 beamline with an in-vacuum undulator, a new toroidal mirror and a cryogenic monochromator. We will briefly describe these developments.

2. The high-flux undulator U17

The straight sections at the ESRF can accommodate three 1.6 m long in-air undulators or two 2.0 m long in-vacuum undulators. The in-air undulators are normally operated at 11.0 mm gap whereas the in-vacuum undulators operate at 6.0 mm. The U17 undulator has been designed for very high flux between 14 and 18 keV at the expense of tunability. The emission at closed gap is dominated by the fundamental at 14.8 keV, but the second and third harmonics are also usable. The strong emission from the first harmonic comes from the fact that the critical energy in the sinusoidal orbit is close to the fundamental energy of the device. The undulator parameters are listed in Table 1. Its spectral flux is 1.9×10^8 photon pulse^{-1} for a 28.2 nC bunch charge (10 mA

Table 1 Undulator parameters on ID09. The (low-beta) source size is 0.117 mm horizontally and 0.024 mm vertically (fwhm). The U17 produces 546 W in the central cone at 200 mA

Period/mm	Poles	Minimum gap/mm	*B*max/T	E_f/keV	E_c/keV	*K*	*P* (W/200 mA)
17	235	6.0	0.544	14.84	13.2	0.86	2740
46	71	16.0	0.643	0.64	15.6	2.76	3116

Table 2 The parameters of the new toroidal mirror

Shape	Cylindrical (in gravity → toroidal)
Dimensions: $L \times W \times H$ (mm^3)	$1000 \times 114 \times 52$
Material	Silicon crystal
Sagittal radius (mm)	71.6
Coating	Pt
Surface roughness (Å; rms)	1.3
Incidence angles (mrad)	2.684
Energy range (keV)	4–34
P = source–mirror distance (m)	33.05
Q = mirror–focus distance (m)	22.37
Demagnification M	0.677
Slope-error (μrad; rms)	0.7 μrad (intensity weighted)
Residual meridional radius (km)*	25.0
Gravity curvature (km)	9.9

operation), see Fig. 1. We believe that this is close to the theoretical limit for an undulator on a third generation machine.

3. The X-ray optics

The layout of the new optics is shown in Fig. 2. The incoming beam is first reduced by the primary slits that remove the diffuse halo around the central cone. The radiation is then passed through the heatload shutter, which relieves downstream components from the heatload of the focused beam. The shutter consists of a rotating copper-block with a tunnel. The shutter is water-cooled and the water runs through the rotation axis. The shutter can open down to 20 ms at a frequency of 3 Hz. The next element is a cryogenic monochromator based on channel-cut silicon 111 crystal. The energy can be varied between 4.0 and 50.0 keV. The orthogonal distance between the crystal surfaces, *i.e*. the crystal gap, is 4.0 mm. The monochromatic beam, which is parallel to the white beam, is shifted upwards by up to 8.0 mm. The next element is a bend cylindrical mirror. The platinum-coated mirror receives the beam at 2.68 mrad, and reflects between 0 and 34 keV. The mirror is placed 33.0 m from the source and the focus is 22.4 m downstream ($M = 0.679$). The sagittal and meridional radius are 71.6 mm and 9.95 km respectively. The mirror is 1000 mm long, 114 mm wide and 52 mm thick. These dimensions have been chosen so that the gravity-bend mirror is close to an ideal toroid. A stepper motor pushes from below the mirror and fine-tunes the curvature. The intensity distribution and figure errors along the mirror are shown in Fig. 3. The

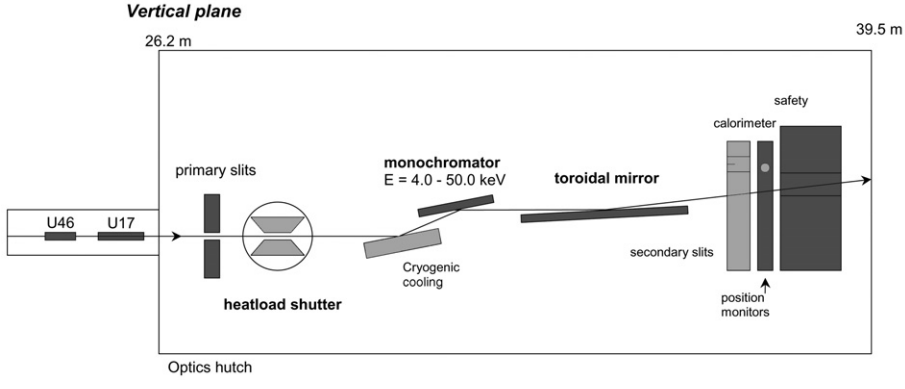

Fig. 2 Layout of the optics hutch on beamline ID09B.

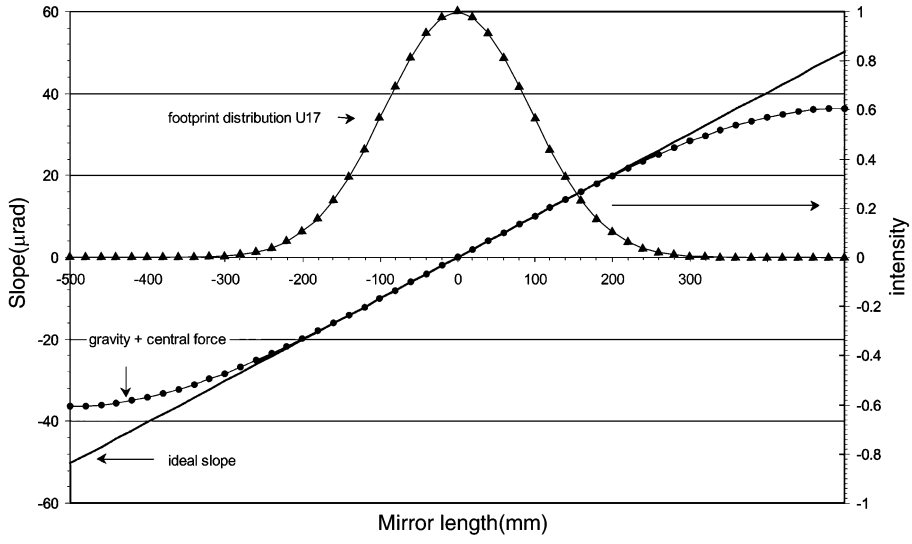

Fig. 3 The intensity distribution on the toroidal mirror from the U17 undulator (–▲–). The mirror receives the beam at an angle of 2.68 mrad. The slope produced by gravity and the (compensating) central force is shown (–●–). The theoretical slope, parabolic in shape, is shown (—). The figure error in the zone from −200 to +200 mm is less than 0.1 mrad.

ideal slope profile, corresponding to a parabolic shape, is a straight line. Note that the deviation from the straight line is below 0.1 μrad between $-200 < x < 200$ mm. The slope error of the optical surface of the cylindrical mirror is specified to be less than 0.7 μrad (rms) in the 400 mm central zone. In the absence of vibrations, the vertical focal size should thus be as small as 75 μm (fwhm). Note the vertical size is determined solely by the slope error! We are aiming at a tight vertical focus to optimize the transmission in the chopper in 16-bunch mode, where the tunnel height has to be as small as 145 μm to produce an opening window around 0.3 μs. The mirror is loaded with 546 W of beam of which 134 W is absorbed. The heat is extracted laterally by cooling plates that are dipped into indium gallium filled channels running parallel to the optical surface, see Fig. 4. Stress and vibrations from the cooling system are thus eliminated. The measured focal spot

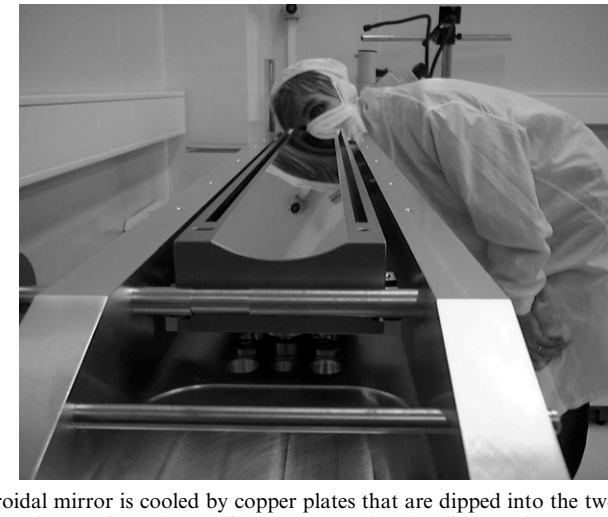

Fig. 4 The new toroidal mirror is cooled by copper plates that are dipped into the two indium–gallium filled channels. Vibrations and stress from the cooling system are hereby eliminated.

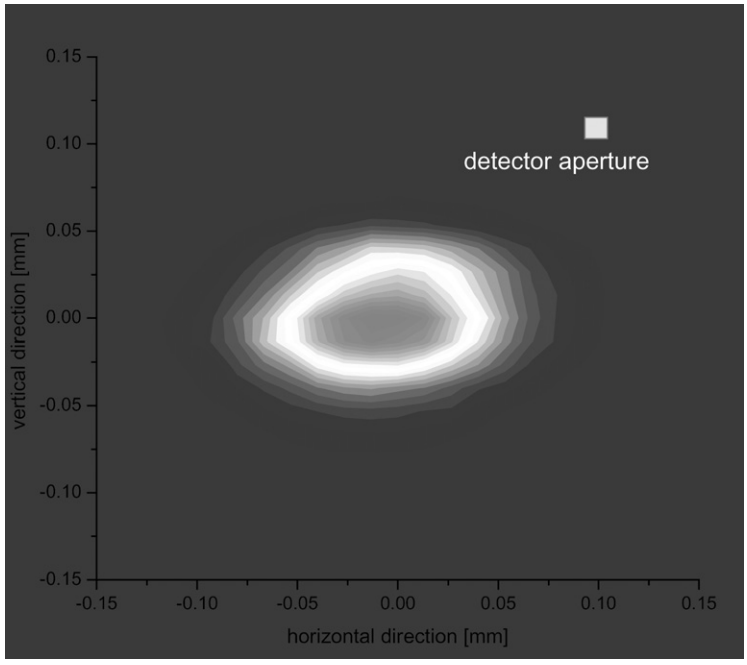

Fig. 5 Polychromatic focus of the U17 undulator produced by the toroidal mirror in Fig. 4. The focus is 0.100 mm horizontally and 0.070 mm vertically.

Table 3 Flux numbers for pump and probe experiments

Beamline configuration	Single-shot flux/ photon (10 mA pulse)$^{-1}$	Flux at 896.6 Hz/ photon s^{-1} (10 mA)$^{-1}$
Si(111) + toroidal mirror	2.4×10^7	2.2×10^{10}
Multilayers + toroidal mirror	1.7×10^9	1.5×10^{12}
Toroidal mirror	1.1×10^{10}	9.6×10^{12}

is shown in Fig. 5. The flux values of the new beamline are summarized in Table 3. The important number for Laue diffraction is the photon integral per pulse. By contrast, for diffraction experiments on a circulating liquid, it is the stroboscopic flux per second. The flux level from an ESRF bending magnet, monochromatised by silicon 111, is 5×10^9 photon s^{-1}.

4. The single-bunch chopper

The chopper consists of a triangular rotor made of titanium, which rotates about its centre of gravity. The rotation axis is horizontal and perpendicular to the beam. The rotor has a groove in one of its sides. The groove is covered (or roofed) by small plates at its extremities. The groove is thus made into a semi-open tunnel. The rotor, which is suspended in magnetic bearings, rotates at 896.6 Hz, which produces a supersonic speed of 545.3 m s^{-1} at the tips of the rotor. It is thus mandatory to keep the rotor in vacuum. The 896.6 Hz frequency is the 396th sub-harmonic of the orbit frequency of the storage ring. The chopper is shown schematically in Fig. 6 and its parameters are summarised in Table 4. The rotor speed is controlled by a feed back which stabilises the rotor to an accuracy $\delta\omega/\omega$ of 1×10^{-5}. The frequency has been limited to 896.6 Hz since the rotor shaft has a resonance at 998 Hz and breaks down from the centrifugal force at 1300 Hz. The opening window, *i.e.* the transmission *versus* time, is generally trapezoidal in shape.

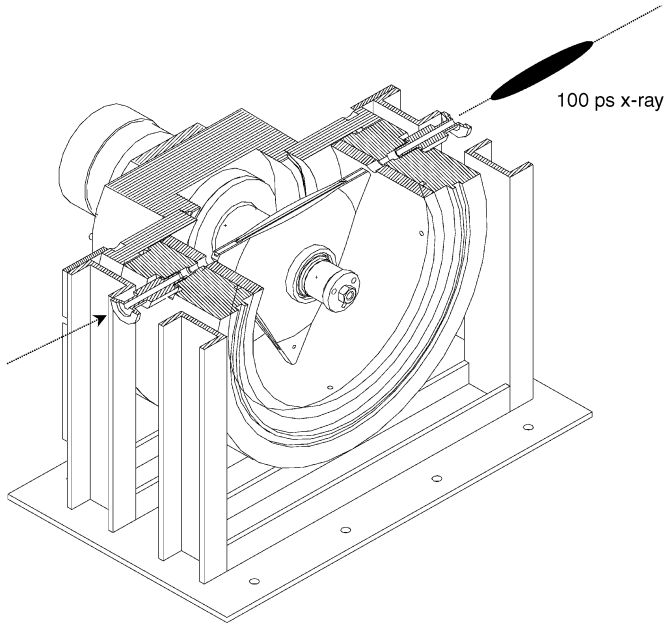

Fig. 6 The chopper for single-pulse selection. The rotor is synchronized to the bunch clock.

Table 4 The chopper parameters

Tunnel length (mm)	165.0
Maximum radius (mm)	96.8
Tunnel off-set (mm)	47.35
Minimum frequency (Hz)	10.0
Maximum frequency (Hz)	896.6
Tunnel width (mm)	4.0
Tunnel height (mm)	0.05 to 0.90
Minimum opening: $\delta t_{\min}$ (s)	0.10×10^{-6}
Maximum opening: $\delta t_{\max}$ (s)	0.17×10^{-3}
RMS phase jitter (s)	10.5×10^{-9}

The base line of the trapezoid is:

$$\tau = \frac{a}{2\pi R f \sqrt{1 - (h/R)^2}}$$

where a is the height of the tunnel, R is the maximum radius of the triangle, h is the (orthogonal) distance of the tunnel to the centre of rotation and f is the rotation frequency. $a = 0.70$ mm, $R = 96.8$ mm, $h = 47.4$ mm and $f = 896.6$ Hz gives $\tau = 1.472$ μs. The opening time, at the highest speed, can be varied by having a variable tunnel height. That is done by the use of a trapezoidal tunnel cross-section: the tunnel is 4.0 mm wide and the height increases linearly from 0.05 to 0.90 mm. The opening time can thus be varied from 0.10 μs to 1.89 μs by translating the chopper horizontally. The time between two pulses in single bunch mode is 2.82 μs and it is 0.176 μs in the 16-bunch mode. As the opening window has to synchronise to the centre of three pulses, the opening time has to be slightly shorter than twice the inter-pulse distance. A PC controls the frequency of the chopper and displays the deviation from the desired frequency. This jitter is

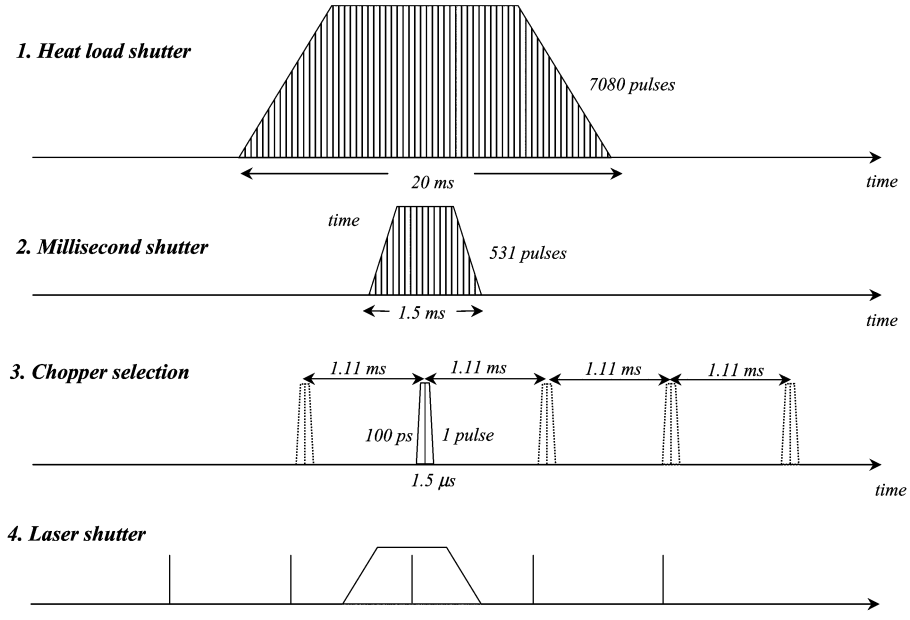

Fig. 7 The synchronization of the four shutters used in single-bunch Laue diffraction. The first shutter, the heatload shutter, allows one to load the focused white beam on the (uncooled) chopper.

recorded every two minutes; it is typically 10.5 ns (rms) at full speed. The synchronisation of the open position is based on a phase shifted reference clock at 896.6 Hz, which also controls the cavity dump in the femtosecond laser. The sampling of the pick-up signal from the chopper is done at 44.02 MHz(RF/8).

The chopper selects pulses continuously at 896.6 Hz giving a pulse on the sample every 1.11 ms. The femtosecond laser also runs at 896.6 Hz and by moving it relative to the fixed X-rays, one can probe photosensitive systems in a pump/probe fashion to about 100 ps resolution. However, there are not many bio-crystals that can tolerate a laser running at 896.6 Hz. In the case of Laue diffraction on myoglobin, hemoglobin and PYP, the laser repeat frequency is normally slower than 1 Hz. For these *slow repeat* experiments, the chopper and femtosecond laser are gated by two millisecond shutters. The X-ray ms-shutter is installed in vacuum upstream of the chopper. It consists of a 60 mm long bar with a tunnel along its length. The tunnel cross section is also trapezoidal: it is 5 mm wide and the height increases from 0.3 to 2.0 mm. The tunnel is positioned on the axis of rotation. The tunnel-bar is rotated by a stepper motor that is mounted in air. The shortest opening time is 0.2 ms, which is obtained by accelerating the tunnel from $-90°$ to $+90°$. It takes 48 ms to move from $-90°$ to the open position at $0°$. The laser shutter is a commercial UniBlitz shutter, which can open down to 1 ms. The timing of the four shutters is shown in Fig. 7.

5. The femtosecond laser for reaction initiation

The femtosecond laser is used to initiate photoreactions and to trigger a jitter free streak camera. The laser comprises four stages. The first stage is a continuous wave (CW) diode-pumped laser from Coherent (VERDI). It produces 5 W of frequency-doubled light at 532 nm. The VERDI pumps a Ti: sapphire crystal in the MIRA femtosecond laser from Coherent. The optical cavity in this laser runs in phase with the RF clock at RF/4(88.05 MHz). This oscillator produces, *via* the Kerr-effect in the Ti: sapphire crystal, weak 100 fs pulses at 800 nm. The frequency is adjusted to RF/4 by adjusting the length of the cavity. The third stage, the Hurricane Laser from Spectra Physics, is a chirped pulse amplifier (CPA) which stretches, amplifies and compresses a sub-train of pulses at 896.6 Hz. The pulses are amplified to 1.1 mJ pulse^{-1} at 800 nm and the pulse duration is

130 fs. The laser system is phased to the X-rays in the following way. First the X-ray chopper is centred on a single bunch which produces a train of 100 ps X-ray pulses at 896.6 Hz. The MIRA oscillator will now have a pulse that is less than half a period away (5.7 ns). By shifting the phase of the 88.05 MHz reference clock, the two pulses can be put into coincidence. This pulse needs to be amplified at 896.6 Hz. The starting point is to use the phase from the chopper and then fine-tune the delays for the seed, the pump and the cavity dump. There are two reference signals: a bunch clock at 352.201 MHz and a single-bunch clock at 355.042 kHz. The single-bunch clock marks the position of the bunch in single-bunch mode. From that we divide by 396 to get to the chopper frequency of 896.6 Hz. Now the precise phasing of the chopper requires a phase-shift, which has to be determined experimentally. A Stanford delay generator (DG535 no 1) generates the delay, which is a machine constant. Once determined, the chopper will automatically phase with the single bunch.

The fourth stage in the laser is the optical parametric generation (OPG)/optical parametric amplification (OPA), which uses frequency mixing to obtain wavelengths between 460 and 760 nm. It can produce 20–30 μJ per pulse.

From Table 4 it is seen that the laser can produce more than 3×10^{13} photon pulse^{-1}. That is comparable to the number of unit cells in a (100 μm)^3 myoglobin crystal. It is thus possible, at least in principle, to excite such a crystal to a very high degree. In practice one would like to have 5–10 times more photons to compensate for losses between the laser and the sample. The laser is focused by a lens that is mounted on an (x, y, z) alignment stage. The focal spot can thus be scanned into a pinhole on the sample goniostat.

The timing between the laser and the X-rays is measured using a GaAs photoconductor with a fwhm resolution of 50 ps.[10] The signal is recorded on a 3 GHz oscilloscope from a Tektronix TDS 694C. The setting of time zero is defined to an accuracy of ±10 ps which is sufficient for the 60 ps resolution of the set-up.

Finally we note that very short laser pulses have a finite bandwidth. For a Gaussian pulse shape, the relation between pulse width and bandwidth is:

$$\Delta\nu\Delta t \; > \; 0.441$$

Let us consider a 100 fs pulse at 800 nm as an example. The frequency is derived from $\Delta\nu = c$, which gives $\nu = 3.75 \times 10^{14}$ Hz. Consequently $\Delta\nu/\nu = \Delta\lambda/\lambda = 1.2\%$. This distribution tends to smear out the excited state for very short pulses.

6. The recombination of molecular iodine in CCl_4

As an example of a pump and X-ray probe experiment in a dilute disordered sample, we will measure the X-ray scattering from excited I_2 and describe results following the model developed by Harris.[11] More recently Savo Bratos *et al.* have worked out a theory for ultrafast X-ray scattering in the presence of a laser excitation and applied this theory to molecular iodine.[12] The potential energy of two iodine atoms is shown in Fig. 8. The ground state X-curve is shown with the first two vibrational levels. For a Morse potential, the vibrational levels are[13]

$$E_{\mathrm{vib}} \; = \; (\nu \; + \; 1/2)\omega_{\mathrm{e}} \; - \; (\nu \; + \; 1/2)^2\omega_{\mathrm{e}}\chi_{\mathrm{e}}.$$

where ω_{e} is the eigenfrequency and x_{e} is a constant derived from the Morse potential. For he first level ($n = 1$), the zero point motion, is 26.52 meV and for the second ($n = 2$) 79.56 meV. The thermal occupancy is determined by the Boltzmann factor $g = \exp(-\Delta E_{\mathrm{vib}}/kT)$. At 300 K the ground and first excited state are 64.9% and 23.4% populated respectively. This leads to dispersion in the excited state. The optical absorption band is shown in Fig. 9.

In our experiment, the molecule is excited vertically to the B-state by a 150 fs pulse at 2.340 eV (530 nm). Note however that the second vibrational level is sent to the $^1\pi_{\mathrm{u}}$ state. A calculation of the Franck–Condon factors, shows that the B and the $^1\pi_{\mathrm{u}}$ state are excited in the ratio 5.18 : 1 respectively.[14] Both curves are repulsive and the molecule moves apart at increasing speed. At the curve crossing between B and $^1\pi_{\mathrm{u}}$, the B molecules may cross to $^1\pi_{\mathrm{u}}$ from where it continues to expand until they reach the liquid boundary at 4.5 Å. Some molecules remain in the B-state after the first passage of the curve crossing. After one full oscillation they return to the crossing and

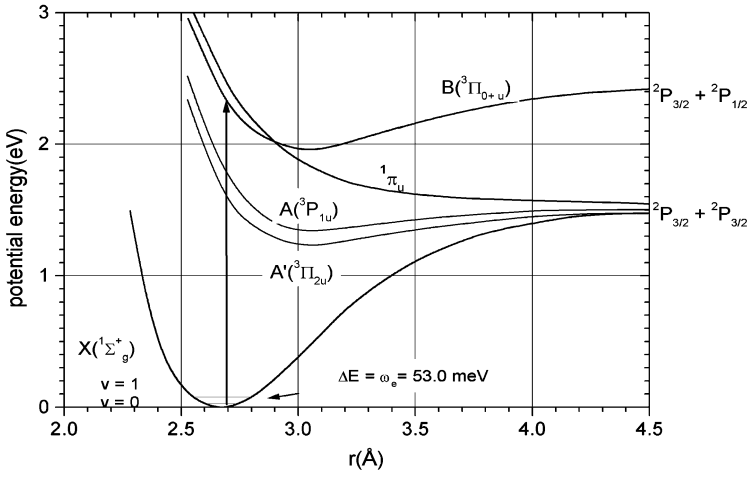

Fig. 8 The potential energy of the iodine molecule for different wavefunctions X, A/A′ *etc*. The molecule is dissociated by a 150 fs pulse at 530 nm that excites the molecule to the B state (vertical arrow).

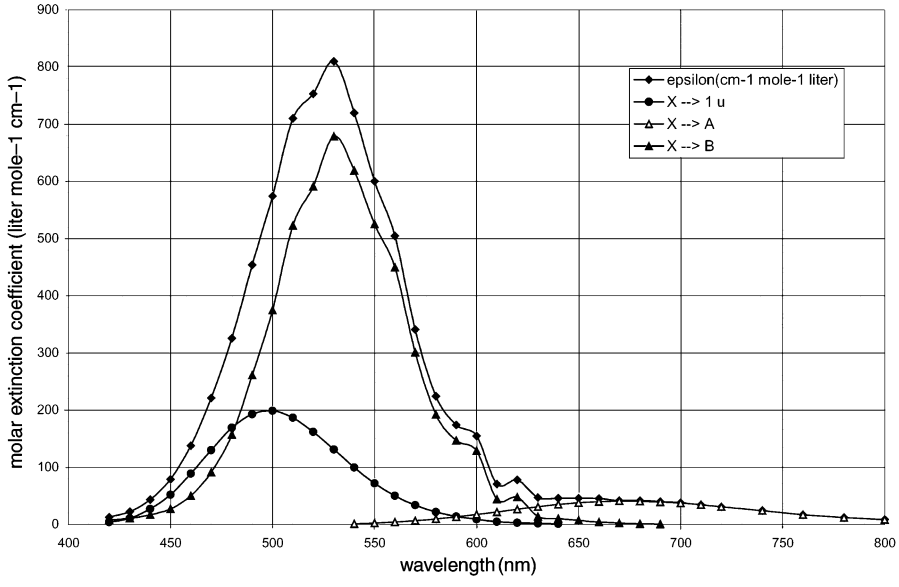

Fig. 9 The molar extinction coefficient of iodine (after Tellinghuisen). The partial absorption to the 1u, A and B branches is also shown.

dissociate at a certain probability. After a few oscillations lasting 1–2 ps, the B-state is depleted. The solvent molecules surrounding the hot atoms form a cage that more or less traps the atoms and then catalyze the recombination process. However, a solvent molecule may slide in between and force them to separate. The probability of cage escape depends on the viscosity of the solvent and varies between 30 and 90%. The separated atoms recombine diffusively in microseconds. The information about the solvent cage from optical spectroscopy is limited and X-ray scattering may eventually be used to measure the size of the cage at the different stages in the recombination. The in-cage atoms recombine diffusively in 1–10 ps and form I_2* on the A/A′ or X curve. Collisions

with the cage cool the molecules and the molecule relaxes towards the potential minima on the X, A or A′ curves. Molecules on the X potential thermalise in 50–200 ps by transferring energy to the solvent. The A/A′ molecules thermalise in about 10 ps to a new stable position at 3.1 Å. This process is faster than the X cooling due to the lower energy transfer. The lifetime of the A/A′ state depends on the polarity of the solvent; it varies from 60 ps in alkane solvents to 2.7 ns in CCl_4. The Franck–Condon factors for a vertical transition $A/A' \rightarrow X$ are low and it is believed that the A/A′ molecules decay to the ground state through collisions with the solvent that stretches the molecule to the cage boundary where the energy-gap to the ground state is small. That enables the molecule to curve cross to the ground state.[15,16] To summarize the picture developed by Harris, the molecules recombine in four processes:

1. Vibrational cooling along A/A′ in 10 ps.
2. Vibrational cooling along X in 50–200 ps
3. Intersystem crossing from A/A′ to X in 60–2700 ps.
4. Non-geminate recombination in μs.

With the exception of process 2, synchrotron experiments can resolve these processes.

7. Experimental configuration

The diffuse scattering was recorded on a MARCCD detector, which was centered on the incident beam. The iodine was dissolved at 20 mM in CCl_4 *i.e.* the ratio of I_2 to CCl_4 was 0.0019. The liquid was injected into the joint focus between the X-rays and the laser in a 0.3 mm diameter capillary, see Fig. 10. The capillary was used to make the flow stable and to avoid fluctuations in the vapor pressure. The iodine was excited with yellow light (580 nm) from a nanosecond laser. The pulse width was 2.2 ns, which became the time-resolution of the experiment. At this wavelength and concentration, the optical absorption μ^{-1} is 1.0 mm.[14] The laser beam was focused to 0.7×1.0 mm^2 and the incident energy was 9.0 mJ pulse^{-1}. The X-rays were delivered by the single-line undulator U20 and the synchrotron was operated in single-bunch. The spectrum of the U20 has one harmonic at 16.45 keV and its bandwidth is 2.37%. The increase in flux, as compared to a conventional monochromatic beam from a Si(111) monochromator was 460! The beamsize on the sample was 0.20 mmh $\times$ 0.32 mmv and the flux 3.2×10^8 photon pulse^{-1} for a 10 mA bunch. The experiment was repeated at 10 Hz and the liquid exposed for 100 s per time delay. The data were collected in pairs of *laser on* and *laser off* for every time point. The Ø132.5 mm detector was positioned 40 mm

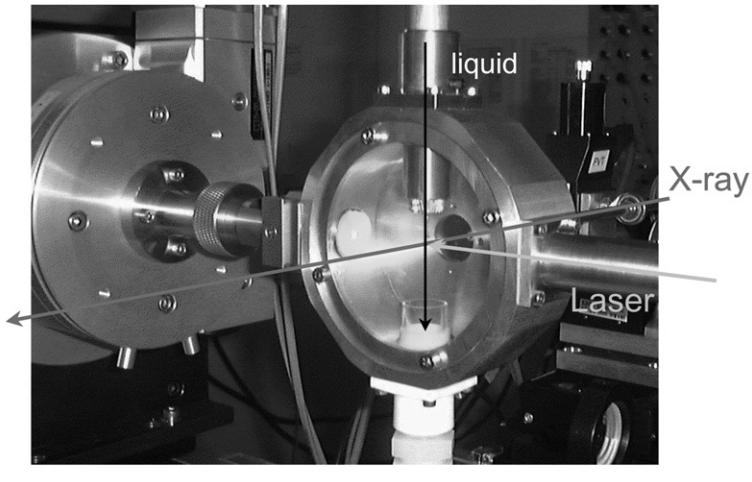

Fig. 10 Sample chamber for liquid experiments. The liquid enters from above and is collected in a funnel below the interaction point. The pumping speed is set such that the sample is replaced between two pulses (1.1 ms apart). The scattering pattern is collected on a CCD detector centered on the incident beam. Cell designed by Armin Geis (ESRF).

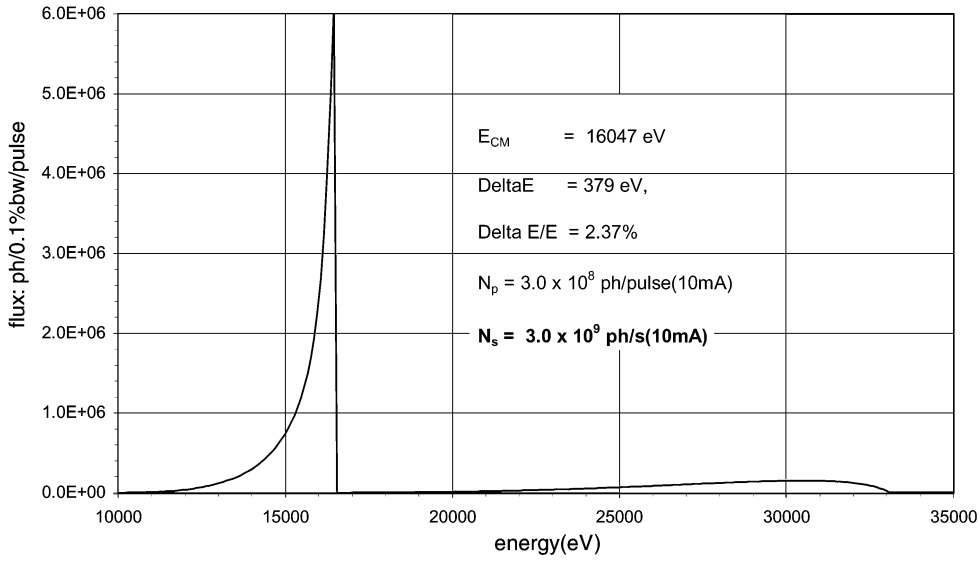

Fig. 11 The spectral flux in one pulse from the single-line undulator U20. The second harmonic is neglected in the analysis.

from the jet and the 2θ-angle was recorded between 2.05° and 58.55°. The corresponding Q-range was 0.29–7.94 Å, which is calculated for a center of mass wavelength of 0.774 Å. The spectrum of the U20 undulator is shown in Fig. 11.

8. Experimental observations

The radial distribution from a 100 s exposure of 20 mM of I_2 in CCl_4 is shown in Fig. 12. The data have been integrated radially using the program fit2d, cleaned for cosmic rays and radioactive impurities in the fiber optics and space-angle corrected. The pixel size is 64.689×64.689 μm^2 and

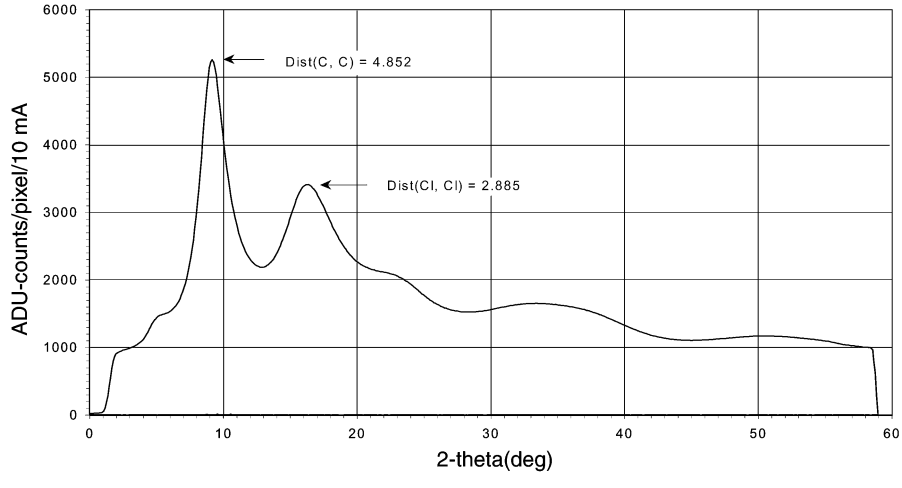

Fig. 12 Radial distribution function for 20 mM I_2 in CCl_4 without laser excitation.

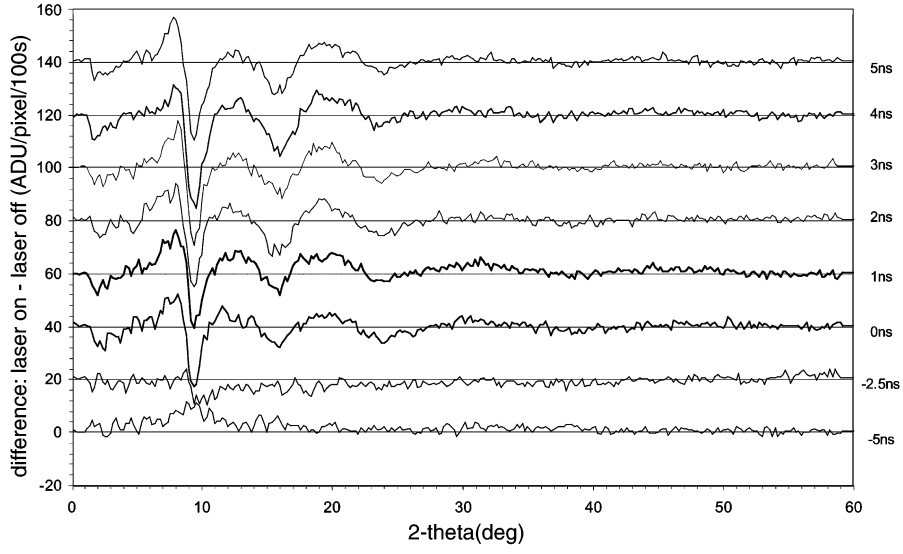

Fig. 13 Difference maps for time delays between −5 ns and 5 ns. The exposure time was 100 s and the integral flux: 3×10^{11} photons.

the software corrects the counts making the pixel perpendicular to the 2θ scattering angle at a distance of 40 mm. Note the oscillatory nature of the (dominating) solvent scattering. The main peak is found at 9.25°, which represents the distance between two CCl_4 molecules, *i.e.* it corresponds to a C–C distance of 4.852 Å. A second peak is seen at 16.45°, which is assigned, to the internal Cl–Cl distance of 2.885 Å in CCl_4.

The difference between frames *laser on* and *laser off* for time points between −5 ns and 5 ns are shown in Fig. 13. The data have been scaled such that the high-angle region oscillates around zero. The first two negative time-points at −5 ns and −2.5 ns are control points used to determine the confidence level of the experiment. In this case the X-ray pulse arrives before the laser and the difference pattern should be zero. The slight peak seen near the solvent peak is possibly due to the trailing edge of the laser pulse that initiates the solvent very slightly. In the high-angle range, the difference curve oscillated below +/−1 ADU per pixel which has to be compared with the liquid background of about 1000 ADU. The difference oscillations are due to the change in I_2 structure and its environment. The high-angle range 25–58°, taken at a delay of 1.0 ns, is shown in Fig. 14. The difference oscillation curve is a mixture of (formfactor) transitions from the ground state to the stretched A/A′-state and from the ground state to atomic iodine. The analysis shows that 78% of the excited molecules are in the A/A-state at 1.0 ns and 22% have broken through the cage. The bondlength of the A/A′-state is found to be 3.14 Å in good agreement with the total-energy calculations in Fig. 9.

The relative number of excited molecules can be determined by scaling the difference oscillations to the high-Q part of the CCl_4 scattering (neglecting the I_2 contribution) which above a Q of 2.5–3.0 Å equals the scattering from free molecules at the solvent density. One finds that 69% of the I_2 molecules are excited. At low angles, the interpretation is more complicated: the photolysis produces an overall temperature rise in the solvent, which, even on the nanosecond time-scale, leads to a small but significant expansion in the CCl_4 to CCl_4 distance. This point is being scrutinized at the moment and we will limit our discussion to a calculation of the temperature rise:

$$\Delta T = \frac{E}{A}\frac{\varepsilon c}{c_p \rho}$$

where E is the energy of the laser flash, A is the illuminated area, ε the molar extinction coefficient, c_p the heat capacity and ρ the CCl_4 density. The values are given in Table 6; they give a ΔT of 4.3 K.

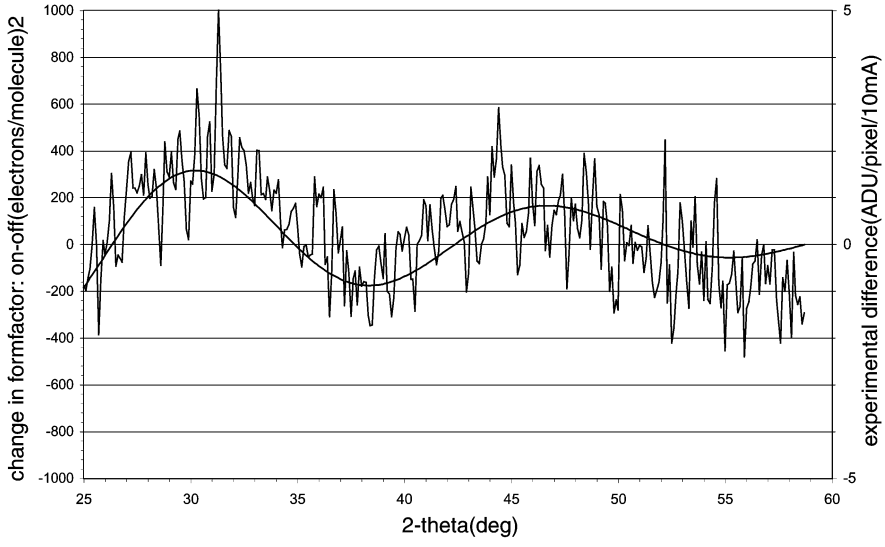

Fig. 14 Difference oscillation from the recombination of iodine. (—) Fit assuming that 78% of the molecules have recombined into A/A′ with a bondlength of 3.14 Å and 22% of the molecules have escaped the cage.

Table 5 The performance of the Ti: Sapphire laser. The pulse length is 150 fs

	Wavelength/nm	Energy/eV	Energy/μJ pulse^{-1}	photon pulse^{-1}	photon s^{-1}
1 harm.	800	1.55	750	3.0E + 15	2.7E + 18
2 harm.	400	3.10	150	3.0E + 14	2.7E + 17
3 harm.	267	4.64	25	3.4E + 13	3.0E + 16
OPG/OPA	460	2.95	35	7.4E + 13	6.6E + 16
OPG/OPA	760	1.63	35	1.3E + 14	1.2E + 17

Table 6 Parameters for the temperature jump in CCl_4

Absorption of iodine at 580 nm	ε	224	cm^{-1} M^{-1}
Thermal capacity of CCl_4	c_p	842	J kg^{-1} K^{-1}
Density of CCl_4	ρ	1590	kg m^{-3}
Concentration of I_2	c	20	mM
Energy of laser flash	E	9	mJ
Laser focus (0.7×1 mm^2 FWHM)	A	0.7	mm^2

Acknowledgement

The authors wish to thank Savo Bratos, Rodolphe Vuilleumier, Fabien Mirloup, Richard Neutze, Armin Geis, Wolfgang Reichenbach, Dominique Block and Peter Trommsdorff and for discussions and assistance on the beamline.

References

1 F. Schotte, *et al.*, in *Third-Generation Hard X-ray Synchrotron Radiation Sources*, ed. Dennis Mills, Wiley, New York, 2002.
2 A. Rousse, *et al.*, *Nature*, 2001, **410**, 65–68.
3 V. Srajer, *et al.*, *Science*, 1996, **274**52931726–9.
4 V. Srajer, *et al.*, *J. Synch. Radiat.*, 2000, **7**, 236–244.
5 V. Srajer, *et al.*, *Biochemistry*, 2001, **40**, 13 802–13 815.
6 S. Techert, F. Schotte and M. Wulff, *Phys. Rev. Lett.*, 2001, **86**102030–2033.
7 R. Neutze, *et al.*, *Phys. Rev. Lett.*, 2001, **87**19195 508-1–195 508-4.
8 A. Geis, *et al.*, *J. Lumin.*, 2001, **94–95**, 493–498.
9 D. Bourgeois, U. Wagner and M. Wulff, *Acta Crystallogr., Sect. D*, 2000, **56**, 973–985.
10 R. Wrobel, *et al.*, *SPIE*, 1998, **3451**, 156–163.
11 A. L. Harris, J. K. Brown and C. B. Harris, *Annu. Rev. Phys. Chem.*, 1988, **39**, 341–366.
12 S. Bratos, *et al.*, *J. Chem. Phys.*, in press.
13 G. Herzberg, *Molecular Spectra and Molecular Structure I. Spectra of Diatomic Molecules.* Robert E. Krieger, Malabar, FL, 1991.
14 J. Tellinghuisen, *J. Chem. Phys.*, 1973, **58**72821–2834.
15 D. F. Kelley, A. N. Abul-Haj and D.-J. Jang, *J. Chem. Phys.*, 1984, **80**94105–4111.
16 J. T. Hynes, R. Kapral and G. M. Torrie, *J. Chem. Phys.*, 1980, **72**1177–188.